Structure
Article

ATP Ground- and Transition States of Bacterial Enhancer Binding AAA+ ATPases Support Complex Formation with Their Target Protein, σ54

Baoyu Chen,[1] Michaeleen Doucleff,[2,3] David E. Wemmer,[2,3] Sacha De Carlo,[4] Hector H. Huang,[4] Eva Nogales,[4] Timothy R. Hoover,[5] Elena Kondrashkina,[6] Liang Guo,[6] and B. Tracy Nixon[7,*]
[1] Integrative Biosciences Graduate Degree Program—Chemical Biology, The Pennsylvania State University, University Park, PA 16802, USA
[2] Department of Chemistry, University of California, Berkeley, Berkeley, CA 94720, USA
[3] Physical Biosciences Division, Lawrence Berkeley National Laboratory, Berkeley, CA 94720, USA
[4] Howard Hughes Medical Institute, Department of Molecular and Cell Biology, University of California, Berkeley, and Lawrence Berkeley National Laboratory, Berkeley, CA 94720, USA
[5] Department of Microbiology, University of Georgia, Athens, GA 30602, USA
[6] BioCAT at APS/Argonne National Lab, Illinois Institute of Technology, 9700 South Cass Avenue, Argonne, IL 60439, USA
[7] Department of Biochemistry and Molecular Biology, The Pennsylvania State University, University Park, PA 16802, USA
*Correspondence: btn1@psu.edu
DOI 10.1016/j.str.2007.02.007

SUMMARY

Transcription initiation by the σ54 form of bacterial RNA polymerase requires hydrolysis of ATP by an enhancer binding protein (EBP). We present SAS-based solution structures of the ATPase domain of the EBP NtrC1 from *Aquifex aeolicus* in different nucleotide states. Structures of apo protein and that bound to AMPPNP or ADP-BeF_x (ground-state mimics), ADP-AlF_x (a transition-state mimic), or ADP (product) show substantial changes in the position of the GAFTGA loops that contact polymerase, particularly upon conversion from the apo state to the ADP-BeF_x state, and from the ADP-AlF_x state to the ADP state. Binding of the ATP analogs stabilizes the oligomeric form of the ATPase and its binding to σ54, with ADP-AlF_x having the largest effect. These data indicate that ATP binding promotes a conformational change that stabilizes complexes between EBPs and σ54, while subsequent hydrolysis and phosphate release drive the conformational change needed to open the polymerase/promoter complex.

INTRODUCTION

Bacteria use many strategies to regulate gene expression. One mechanism that operates at both high efficiency and fidelity is σ54- (σN)-dependent transcription, which permits transcription to range from essentially none to levels high enough to sustain an encoded protein at ~20% of the cellular total (reviewed in Buck et al., 2006). This remarkable dynamic range is achieved in part by features of σ54 that prevent the polymerase/promoter complexes from isomerizing from the closed to the open form (Wang and Gralla, 2001), thus keeping the template strand unavailable for transcription initiation. This is unusual for bacterial RNA polymerase, which normally makes a fast transition from closed to open forms—indeed, most other regulatory mechanisms function by recruiting RNA polymerase or affecting steps after promoter melting. The quiescent σ54-RNA polymerase/promoter complex only initiates transcription when the sigma factor is acted upon by an AAA+ ATPase that functions as a bacterial enhancer-binding protein (EBP), typically bound at DNA sites that are often located well upstream of the promoter. Structural data indicated that two insertions into the canonical AAA+ ATPase fold position the "GAFTGA loop" near the upper rim of the pore in the ring form of the ATPase (Lee et al., 2003). This loop, highly conserved among EBPs, is believed to contact σ54 to couple ATP binding and hydrolysis by the ATPase to a conformational change in the sigma factor (Buck et al. [2006] and references cited therein).

As AAA+ ATPases, EBPs are believed to accomplish this feat by monitoring small structural changes in the active site that are relayed to distant parts of the protein to direct larger scaled conformational changes and accompanying interaction with σ54. Upon binding ATP, a ground-state tetrahedral geometry for the γ phosphate is expected to move through a planar geometry into the transition state for hydrolysis, further evolving into an inverted tetrahedral geometry in the released organic phosphate. "Nonhydrolyzable" ATP analogs (e.g., ATPγS, AMPPNP, AMPPCP, and ADP-berylloflurioide [ADP-BeF_x]) are frequently used to trap the active sites of ATPases in their ground states, and ADP-aluminum fluoride (ADP-AlF_x) is used to trap them in their transition states (see Figures S1A and S1B). Careful use of ATP analogs may thus reveal structural changes in the active site and larger scale conformational changes that are coupled to movement of the GAFTGA-loop region in EBPs.

Previous studies of the EBPs phage shock protein F (PspF) or nitrogen fixation regulatory protein A (NifA) showed that tight binding to σ54 only occurred in the presence of the transition-state analog ADP-AlF_x but not other ATP analogs such as ATPγS, AMPPNP, or ADP (Chaney et al., 2001). Recent structural studies of the ADP-AlF_x state of EBPs alone (De Carlo et al., 2006) or when bound to σ54 (Rappas et al., 2005) locate the GAFTGA loops and σ54 above the surface of the pore of the EBP ATPase domain, consistent with the hypothesis that the GAFTGA loops contact σ54. Recent work suggests that at least one GAFTGA loop may interact with DNA downstream of the promoter (Dago et al., 2007). Structural changes observed upon soaking crystals of apo PspF with AMPPNP to trap the ground state and ATP being slowly hydrolyzed in the absence of Mg^{2+} to access "initial stages of hydrolysis" led to a model for specific interactions that mediate communication between the ATP-binding site and the GAFTGA loops upon nucleotide binding and hydrolysis (Rappas et al., 2006). In the proposed model, events during "initial stages of hydrolysis" stabilize a rotomeric change in the second acidic residue of the Walker B motif (E108 of the $_{107}DE_{108}$ pair in PspF) that drives conformational changes through linkers and secondary structure elements. These changes ultimately extend the GAFTGA loops up and away from the surface of the ATPase so that "at the point of hydrolysis" they can engage σ54. Upon release of hydrolysis product P_i, the Walker B motif rotomer reverts back to its original state, and the GAFTGA loops return to their positions in the ADP-bound state.

Here we report small- and wide-angle X-ray scattering (SAXS/WAXS) data for solutions of the ATPase domain of the NtrC1 protein of *Aquifex aeolicus*, which we call $NtrC1^C$ (the central domain of the three domains of this EBP). The physiological role for NtrC1 remains unknown, but it hydrolyzes ATP and activates transcription from σ54-dependent promoters in *E. coli* (Doucleff et al., 2005). Scattering profiles were obtained for ring forms of $NtrC1^C$ in the apo state as well as when bound to ATP ground-state analogs ATPγS, AMPPNP, or ADP-BeF_x, hydrolysis transition-state analog ADP-AlF_x, or product ADP. The data clearly reveal structural changes, most evident when comparing the apo and ADP states with the ADP-BeF_x and ADP-AlF_x states. The chain-compatible dummy residue-modeling method of Svergun's group (GASBOR [Svergun et al., 2001]) was used with 7-fold symmetry to obtain well-defined structures from the scattering data (such symmetry was seen in the ADP-bound crystal structure of $NtrC1^C$ [Lee et al., 2003] and confirmed in this work for the ADP-BeF_x bound solution conditions by negative-stain electron microscopy). These solution structures show that the ADP-BeF_x and ADP-AlF_x defined ground- and transition states stabilize the GAFTGA loop in a conformation extended up and away from its position in the pore of the ring observed for apo and ADP-bound states. Consistent with this, we also find that both of these analogs stabilize complexes of σ54 with the oligomers of the ATPase domains of NtrC1 and also PspF, as well as with the activated, oligomeric form of full-length NtrC. The ATP ground-state complexes are less stable than the transition-state complexes. Further purified preparation of commercial AMPPNP also supported complex formation between σ54 and $NtrC1^C$, but not to PspF or NtrC. It stabilized structural changes in $NtrC1^C$ that were intermediate between those seen upon binding the metal fluoride analogs versus ATPγS, which did not support binding between σ54 and any of the three EBPs. We thus propose amending the current model (Rappas et al., 2006) for interaction between ATPase and σ54 to one in which ATP binding per se positions the GAFTGA loops to contact the sigma factor, with such contact evolving into a more stable state as hydrolysis occurs.

RESULTS

Concentration Dependence for Oligomerization of $NtrC1^C$

Purified $NtrC1^C$ protein is soluble up to 40 mg/ml, but its oligomeric state is affected by salt concentration. At a protein concentration of 10 mg/ml, we found that the radius of gyration (Rg) estimated from Guinier plots of SAXS data was salt dependent. Raising the concentration of potassium chloride (KCl) from 0 to 200 mM stably reduced Rg from 50.0 Å to about 46.0 Å (Figure S2A). This final Rg is similar to that calculated for a single heptamer of the ADP-bound ring form in the published $NtrC1^C$ crystal structure (44.5 Å, PDB 1NY6). Note that the stacked double ring present in the asymmetric unit of that lattice yields an estimated Rg of 50.5 Å and that centering the two rings as seen for double ring AAA+ ATPases yields an Rg of 49.5 Å. The low salt condition may thus favor stacking two rings. When protein concentration was varied in the presence of 200 mM salt, the Rg values began decreasing at less than or equal to 3 mg/ml (Figure S2B). Dynamic light scattering measurements showed similar results. We conclude that in the presence of 200 mM salt $NtrC1^C$ stably forms a single ring at a protein concentration range of 5 to 10 mg/ml. The scattering studies described below were thus conducted at 10 mg/ml protein concentration and 200 mM KCl. Since binding the ATP transition-state analog ADP-AlF_x has been reported to favor assembly of the related ATPase PspF (Schumacher et al., 2004), we determined its binding properties for $NtrC1^C$ (Hill coefficient of 2.2, apparent K_d of 550 μM; Figure S2C) and measured Rg values for various concentrations of $NtrC1^C$ in the presence of saturating amounts of the analog (Figure S2A). Together with Mg^{2+}, ADP-AlF_x maintained higher Rg values at lower protein concentrations. At higher protein concentrations the analog caused only minor differences in Rg values, consistent with the number of subunits in the oligomer remaining constant in the presence of nucleotide.

SAXS/WAXS Data for Nucleotide-Bound $NtrC1^C$ Rings

SAXS and WAXS data were obtained for apo $NtrC1^C$ in the presence of 5 mM $MgCl_2$, as well as for nucleotide-bound forms in the presence of 5 mM of both $MgCl_2$ and ATPγS,

AMPPNP, ADP-BeF_x, ADP-AlF_x, or ADP at room temperature (as will be explained, different results were obtained for commercial ATPγS and AMPPNP and those which had been repurified by ion exchange chromatography [see Figure S3A]). The 5 mM nucleotide concentration is well above the disassociation constants we found for ATP (194 ± 16 μM; Figure S2D) and ADP-AlF_x (~550 μM) binding to $NtrC1^C$ and the disassociation constants (100–200 μM) reported for nucleotides binding to related bacterial EBPs (Rombel et al., 1999; Wang et al., 2003). Control experiments showed no hydrolysis of AMPPNP and limited (<10%) hydrolysis of ATPγS within the 5 min required for data collection (Figure S3B). The scaled and merged scattering data are shown in Figure 1A (vertically offset for clarity) and Figure 1B (cropped to the Q range of 0.05 $Å^{-1}$ to 0.16 $Å^{-1}$ and scaled to overlap at Q equal to 0.05 $Å^{-1}$). The inset in Figure 1A shows that the error bars are smaller than the line connecting successive data points. Reciprocal space (Q, $Å^{-1}$) is related to the real space (d, Å) by the formula d = 2*π/Q. In this case data spanned the Q range of 0.004 $Å^{-1}$ to 1.24 $Å^{-1}$, or 1570 Å to 5 Å in real space (with the exception of 0.007 $Å^{-1}$ or 900 Å for the lowest angle data for the ADP-BeF_x and repurified AMPPNP conditions). Clear differences in the scattering curves are evident, most obvious in the Q range of 0.06 $Å^{-1}$ to 0.16 $Å^{-1}$, which reveals changes in the frequency of atom pairs that are separated by 105 Å to 39 Å in real space (Figure 1B). Additional differences are present in the higher resolution data at or above Q of 0.16 $Å^{-1}$. These differences are also evident in the atomic distance distribution functions p(R) that are obtained by Fourier transforms of the scattering data (Figure 1C). The broad and left-centered nature of these plots suggests a flattened disk shape (Svergun and Koch, 2003), and they directly reveal that the AMPPNP-, ADP-BeF_x-, and ADP-AlF_x-bound protein have more atom pairs separated by 35 Å to 65 Å and fewer separated by 80 Å to 110 Å than seen for the other states. The magnitude of the changes is less for AMPPNP, more for ADP-BeF_x, and most for ADP-AlF_x. Such changes were never seen for ATPγS, even when repurified, and most readily observed for AMPPNP when it was further purified. The p(R) functions slowly approach zero by ~180 Å, providing direct estimates of the maximum diameters (D_{max}) for the ATPase particles. Guinier plots (Figure 1D) display linear scattering devoid of any hints of aggregates or particle interference (Glatter and Kratky, 1982). The slopes of the Guinier plots yield Rg values of 45.6 ± 0.1, 44.3 ± 0.1, 45.2 ± 0.1, 44.3 ± 0.1, 43.1 ± 0.1, 45.4 ± 0.1, and 45.6 ± 0.1 Å for apo, repurified ATPγS, commercial AMPPNP, repurified AMPPNP, ADP-BeF_x, ADP-AlF_x and ADP conditions, respectively.

$NtrC1^C$ Forms Heptamers in Solution

Ab initio structure determination from SAXS/WAXS data is an ill-posed problem and in this case required that we apply a priori knowledge of the oligomeric state. To determine the number of subunits in the assembly, we collected electron microscopy images of $NtrC1^C$, confirming that the heptamers seen in the crystal structure of $NtrC1^C$

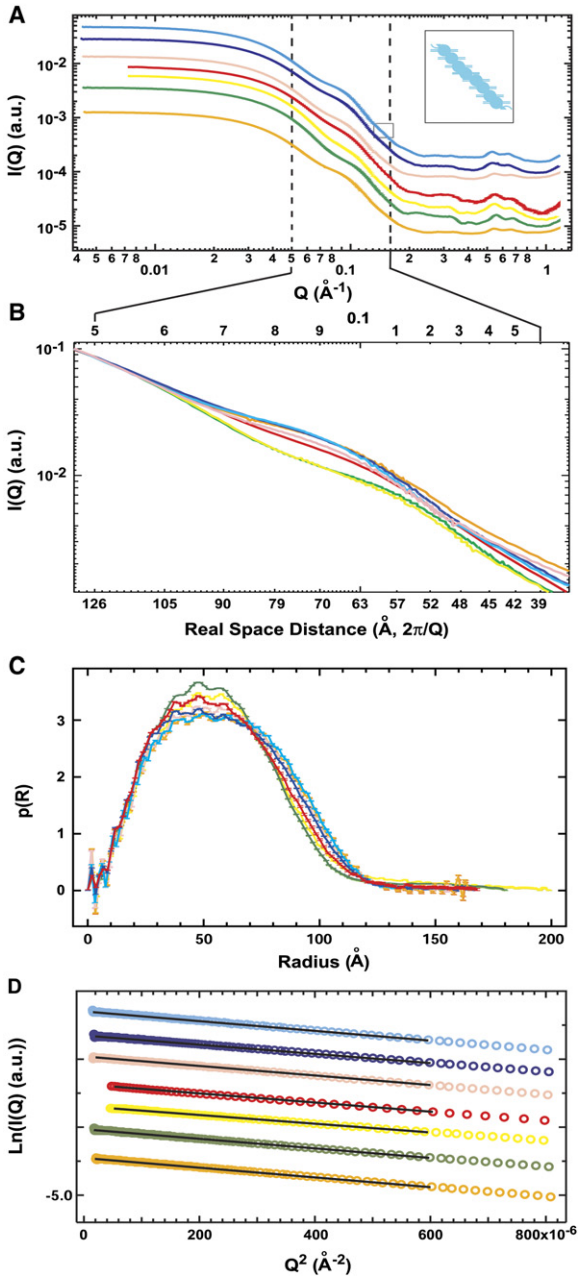

Figure 1. Combined SAXS/WAXS Data for $NtrC1^C$ in Various Nucleotide States

(A–D) (A) Scattering profiles (average and standard deviation of 10 repeated measurements are arbitrarily offset for clarity; enlarged in inset); (B) the dashed region in (A) scaled to identical intensity at Q = 0.5 $Å^{-1}$; (C) p(R) functions (normalized to a common total probability, with standard error of the data in [A] propagated through the inverse Fourier transform implemented in GNOM); and (D) Guinier plots for $NtrC1^C$ with 5 mM $MgCl_2$ (cyan), or with $MgCl_2$ plus 5 mM ATPγS (blue), AMPPNP (pink), repurified AMPPNP (red), ADP-BeF_x (yellow), ADP-AlF_x, (green) or ADP (orange).

(Lee et al., 2003) are relevant to the solution state and are not an artifact of crystal packing. The concentration of protein needed to sustain rings, even when stabilized

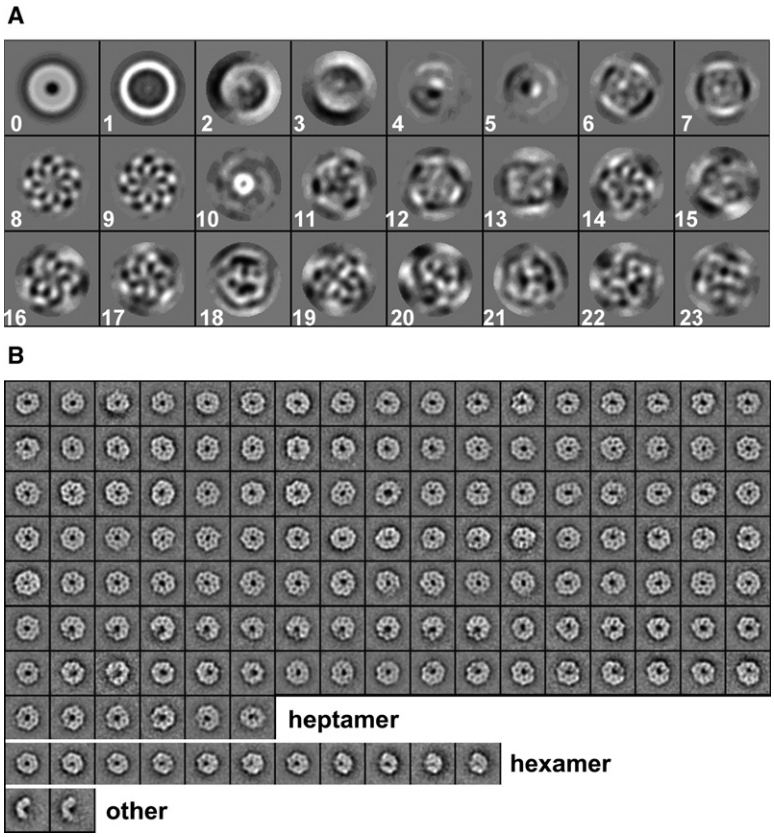

Figure 2. Negative-Stain EM Images of NtrC1^C Bound to ADP-BeF$_x$

(A and B) (A) Eigenimages after the first round of reference-free translational alignment (no symmetry or rotational alignment) and (B) class averages from the full data set, representing 87% heptamers, 11% hexamers, and 2% other forms. The number of raw particles contributing to each class average is not indicated and may vary.

with ADP-AlF$_x$ or ADP-BeF$_x$, was too high for directly adsorbing to a carbon film support. We therefore used glutaraldehyde crosslinking to maintain the ADP-BeF$_x$-bound oligomer even when diluted to 0.6 mg/ml (Figure S4). Under optimal crosslinking conditions, we observed intact particles forming well-defined rings and a few other smaller particles that likely represent NtrC1^C subunits that had not undergone full assembly or were not fully crosslinked and disassembled during the dilution and staining processes. Semiautomatic particle-picking procedures yielded 17,898 molecular views. The eigenimages (Frank et al., 1996) that resulted from translational alignment only and classification using a large number of factors to avoid bias clearly showed 7-fold symmetry (see orders 6–9, Figure 2A). This first classification produced class averages representing mainly heptamers, some hexamers, and smaller particles. Four subsequent rounds of multivariate statistical analysis gave a stable classification revealing 87% heptamers, 11% hexamers, and 2% smaller assemblies (Figure 2B).

Solution Models for Nucleotide-Bound NtrC1^C Rings

GASBOR (Svergun et al., 2001) was used with 7-fold symmetry to obtain four sets of eight independent solution structures that best fit the scattering data (Figure S5). Each set differed in the D_{max} value used to determine the p(R) function, which together sampled a 20 Å range centered on the optimal values shown in Figure 1C. The normalized spatial discrepancy (NSD) criterion of SUPCOMB (Kozin and Svergun, 2001) was used to generate pairwise comparisons of the individual solutions for the different nucleotide states. The ADP-BeF$_x$ and ADP-AlF$_x$ structures clearly formed a unique group. Less dramatic clustering was evident for two additional groups containing either the Apo and ADP structures, or the ATPγS and AMPPNP structures (Figure S6).

The filtered, averaged structure for each nucleotide state is displayed in Figure 3 as solvent-excluded surfaces (3.4 Å probe). For comparison, the ADP-bound crystal structure is superimposed on each surface (movies sequentially overlaying these surfaces are available online in the Supplemental Data). Several structural features are evident, with the models differing in three major ways: (1) by the display of rounded or pointed protrusions (spikes) of the α-helical domains on the periphery of the ring; (2) by the thickness of the disk; or (3) by the size of the pore openings on the top and bottom portions of the ring. Such structural differences are present even among the ATPγS, AMPPNP, and ADP-BeF$_x$ states, which in principle should all represent the ground state for ATP. Relative to the model for the apo state, that for ATPγS shows a similar thickness, a slightly larger pore, and more clearly defined spikes pointing away from the middle of the ring. The AMPPNP-bound structure is similar to the ATPγS-bound one, but more compact with its spikes moved down from the plane of the GAFTGA loops, leaving

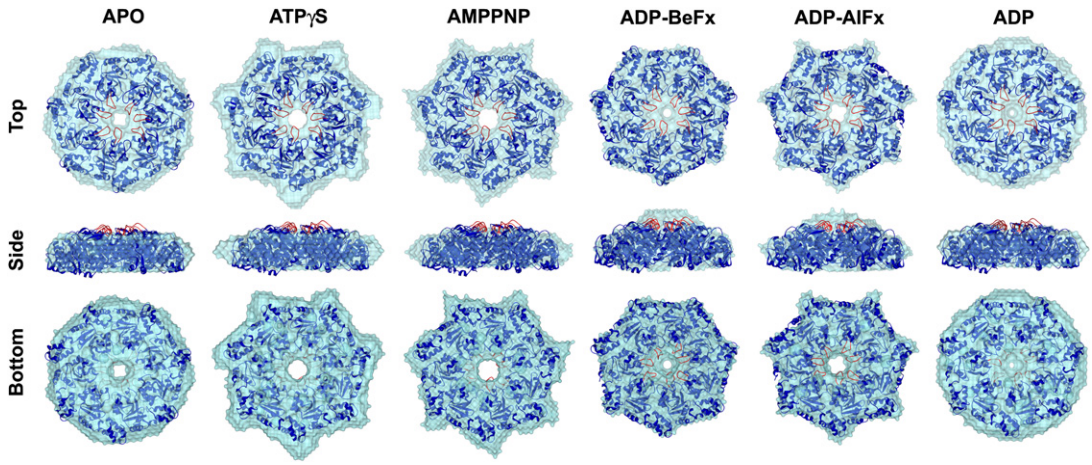

Figure 3. Excluded Volume Surface Models of the NtrC1^C Heptamer
Top, side, and bottom views of the filtered, averaged structure from 32 independently derived, chain-compatible solutions (cyan) for various nucleotide states are shown superimposed on the ADP-bound crystal structure of NtrC1^C (dark blue) with highlighted GAFTGA loops (red).

them a little more exposed above the ring. A very dramatic difference appears in the GAFTGA loop region of the ADP-BeF_x model—it rises further above the plane of the ring. The structure is also much more compact, with its spikes being retracted toward the pore, which is itself more closed on the GAFTGA loop side and more open on the bottom side. The model for the ADP-AlF_x state, believed to represent the transition state for hydrolysis, also shows an elevated GAFTGA loop region but more opened pore (top and bottom sides), with more distinct protrusions from the ring that appear to arise from additional relocations of the α-helical domains (see Movies S1 and S2). This elevated GAFTGA loop region drops back down in the ADP state, and the pinwheel appearance caused by the α-helical domains is lost. The Apo form is likewise round in appearance, but a little more compact and thinner than the ADP-bound form suggesting small changes affecting the pore and location of the GAFTGA loops and α-helical domains.

ADP-BeF_x Stabilizes a Complex between EBPs and σ54

The fact that ADP-BeF_x (ground) and ADP-AlF_x (transition) state analogs supported similar low-resolution structural alterations in the GAFTGA loop region prompted us to revisit the question of which states in the hydrolysis cycle can interact with σ54. We used small-zone gel filtration to monitor the size distribution of the ATPases and sigma factor—in this way a constant presence of nucleotide or analog was maintained. In the presence of Mg^{2+} but absence of nucleotide, the NtrC1^C protein eluted with pseudo-partition coefficient K_{av} of 0.46 ± 0.02, expected for monomers or dimers. Sample dilution (~10-fold) apparently caused the ring to disassemble. The addition of 1 mM ATP, which was significantly hydrolyzed during gel filtration, did not change the elution profile. In contrast to these results, including 1 mM concentration of either ADP-BeF_x (Figure 4A, solid gray curve) or ADP-AlF_x (data not shown) caused the ring to remain stable, eluting with 0.31 ± 0.02 K_{av}. Under these conditions, σ54 protein (solid black curve) eluted with 0.41 ± 0.02 K_{av}. When both proteins were combined in the presence of ADP-BeF_x (dashed black curve) or ADP-AlF_x (data not shown), a new peak eluted with 0.23 ± 0.02 K_{av}, replacing the 0.31 K_{av} peak. Quantitative SDS-PAGE analysis showed the larger material (0.23 K_{av} peak) to be a combination of NtrC1^C and σ54 in a stoichiometry of 6 ± 1 molecules of activator to 1 molecule of sigma factor (at this precision, the measurement is equally consistent with stoichiometries ranging from 5:1 to 7:1). Similar complex formation was also observed when repurified AMPPNP was included in the gel filtration buffer at 1 mM concentration (dashed gray curve and rightmost SDS-PAGE lanes, Figure 4A). A smaller column permitted us to further examine the more expensive AMPPNP and ATPγS nucleotide analogs, confirming a stable association between σ54 and the NtrC1^C ATPase in the presence of repurified AMPPNP (Figure S7A). When not repurified, the extent of this association varied for different commercial lots of the nucleotide. Stabilization of the ring form of the ATPase in the absence of σ54 also varied for these AMPPNP preparations, with the greatest effect seen for the repurifed material (Figure S7A). ATPγS, whether further purified or not, failed to support observable complex between σ54 and the ATPase, although the more pure material did show some ability to stabilize the ATPase ring (Figure S7B).

To determine if these results are generally applicable to other EBPs, the PspF ATPase domain or activated, full-length NtrC protein was subjected to gel filtration chromatography together with σ54 in the presence of ADP-BeF_x (Figures 4B and 4C) or ADP-AlF_x (data not shown). Both analogs supported complex formation between these ATPases and σ54. Unlike NtrC1^C, these EBPs did not form complexes with σ54 when repurified AMPPNP was present in the chromatography buffer; like NtrC1^C, they failed to form complexes when ATPγS was present (data

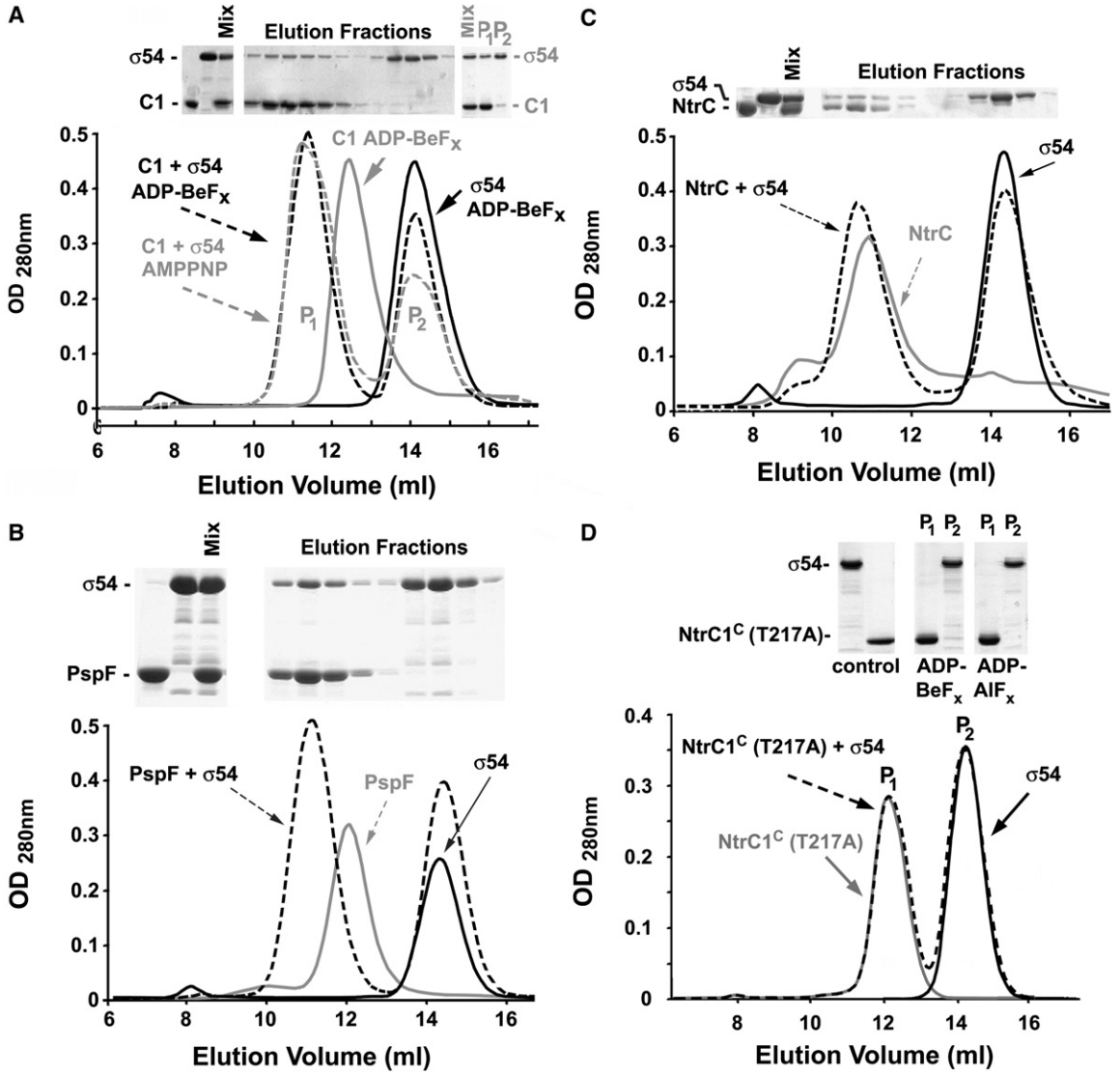

Figure 4. ADP-BeF_x and AMPPNP Stabilize a GAFTGA-Loop-Dependent Complex of σ54 with the ATPase Domains of NtrC1 or PspF, or the Full-Length Activated Form of NtrC

(A) Size-exclusion chromatograms developed in the presence of ADP-BeF_x or AMPPNP for $NtrC1^C$ alone (solid gray line), σ54 alone (solid black line), or a mixture of the two with excess σ54 (dashed black and gray lines) are aligned below SDS-PAGE analyses of (left to right) the purified proteins, the loading mixture, elution fractions for the ADP-BeF_x experiment (aligned with the chromatogram), and the loading mixture and aliquots of peaks P1 and P2 for the AMPPNP experiment.

(B–D) The experiment was run as for ADP-BeF_x in (A), but in the presence of (B) the ATPase domain of PspF, (C) the full-length form of NtrC (S160F, 3Ala) activated by binding Mg^{2+}/BeF_3^-, and (D) the T217A substitution variant of $NtrC1^C$ in both ADP-BeF_x and ADP-AlF_x conditions (for [D], only fractions for peaks P1 and P2 were analyzed by SDS-PAGE).

not shown). These data show that, although the three activators respond to different ground-state analogs in different ways, they all consistently bind to σ54 in the ground state mimicked by ADP-BeF_x.

The ADP-BeF_x- or AMPPNP-Stabilized Complex Requires the GAFTGA Loop

The threonine side chain in the GAFTGA loop has been shown to be crucial for complex formation between ATPase domain and σ54 (Chaney et al., 2001). We substituted residue T217 of the $G_{214}AFTGA_{219}$ loop of the $NtrC1^C$ ATPase with alanine. The mutationally altered protein was purified as readily as the wild-type. Dynamic light scattering, size-exclusion chromatography, and ATP hydrolysis assays showed that it formed rings in a similar concentration-dependent manner (saturating at ≥5 mg/ml) and hydrolyzed ATP with a similar turnover rate (15 μM ATP per μM dimer equivalent per min at 21°C). Adding 1 mM ADP-BeF_x or ADP-AlF_x to the chromatography buffer stabilized the ring form of the variant

ATPase and promoted structural transitions evident in SAXS data similar to those seen for the wild-type protein (Figure S8). Despite these normal attributes of the substitution variant, it failed to coelute with σ54 when they were cochromatographed in the presence of 1 mM concentrations of either ADP-BeF_x, ADP-AlF_x (Figure 4D), or repurified AMPPNP (data not shown).

ADP-AlF_x Stabilizes Ring and Complex with σ54 More Strongly Than Does ADP-BeF_x

Knowing that formation of $NtrC1^C$-σ54 complexes in the presence of both the ADP-BeF_x ground- and ADP-AlF_x transition-state analogs depended upon an intact GAFTGA loop, we performed several experiments to determine if they are essentially the same complex, or are distinct complexes. Large-zone gel filtration (Nenortas and Beckett, 1994; Valdes and Ackers, 1979) showed that assembled rings of $NtrC1^C$ are less stable in the presence of ADP-BeF_x than in the presence of ADP-AlF_x, but the measurements could not be performed at low enough concentrations to monitor disassociation of complexes with σ54 (Figure 5A). Also, as previously shown for the PspF ATPase (Chaney et al., 2001), incubating the $NtrC1^C$ ATPase together with σ54 and ADP-AlF_x gave complex with the sigma factor that persisted during native polyacrylamide gel electrophoresis despite the absence of the nucleotide analog from gel and buffer (Figure 5B). A much smaller amount of complex formed in the presence of ADP-BeF_x also survived such electrophoresis (Figure 5B). As expected from prior studies (Chaney et al., 2001), this assay showed stable complex for PspF and σ54 when they were preincubated in the presence of ADP-AlF_x, and no complex was evident when the proteins were preincubated with ADP-BeF_x (data not shown). However, including the AlF_x or BeF_x metal fluorides and ADP in the gel and electrophoresis buffer not only gave rise to complex formation with σ54 in both states, but also clearly showed that ADP-AlF_x has a greater stabilizing effect on PspF rings and its complex with σ54 (Figure 5C).

DISCUSSION

Data from small- and wide-angle solution scattering, electron microscopy, and molecular biological experiments reveal a complex of the $NtrC1^C$, NtrC, and PspF AAA+ ATPases with their target protein, σ54, under conditions previously thought not to support stable complex formation. The current model for the mechanism of EBP action maintains that the GAFTGA loops stably engage σ54 at the transition state for ATP hydrolysis (Rappas et al., 2006). This model was based on the seminal observations of Chaney and coworkers showing that complexes could be observed in the presence of ADP-AlF_x but not ATPγS, AMPPNP, or ADP (Chaney et al., 2001). The data that we present are largely consistent with those prior observations; however, we observed that AMPPNP stabilizes a complex between $NtrC1^C$ ATPase and σ54. This was also true for the analog ADP-BeF_x, which was not described in the previous studies. We interpret these observations as evidence for a novel complex between EBP and σ54 that is stabilized by the ground state of ATP.

Our interpretation rests on several considerations. First, it is commonly believed that the AlF_x moiety in ADP-AlF_x has a planar geometry like that of an ATP transition state while the "γ-phosphate" of the analogs ATPγS and AMPPNP and the BeF_x moiety in ADP-BeF_x have a tetrahedral geometry like that of an ATP ground state. An alternative hypothesis is that in the context of the EBP ATPase active site the ADP-BeF_x analog also mimics the transition state for ATP hydrolysis. We favor the former hypothesis rather than the latter one. The original report on using the metal fluoride ADP analogs argues that the geometry of the fluorides in the BeF_3^- and BeF_4^{2-} complex ions is consistently tetrahedral (Chabre, 1990). A survey of 96 crystal structures containing BeF_x or AlF_x (see Table S1) shows that 34 of 34 BeF_x moieties are in strict tetrahedral conformation (thus ground-state analogs) and 58 of 62 AlF_x moieties are in strict planar quadrangular or trigonal conformation (thus transition-state analogs). Three of the 62 AlF_x moieties were in a slightly skewed planar conformation (still proposed by the authors to represent transition-state mimics). Only 1 AlF_x moiety was in a tetrahedral conformation (but presented as a mimic of an intermediate in a phosphoryl-group transfer reaction). Second, it is not uncommon for some ATP analogs to "work better" for a given protein. Our data clearly show differences in the response of $NtrC1^C$ to ATPγS, AMPPNP, and ADP-BeF_x, and in their respective abilities to support complex formation with σ54. Also, the three EBPs we studied differed in their response to AMPPNP, the quality of which varied from lot to lot and was improved by repurification. We integrate these two sets of considerations by presuming that ADP-BeF_x, AMPPNP, and ATPγS are each functioning as a tetrahedral ground-state analog, but that the ATPase active sites sense differences in their atomic compositions. Similar variability was observed for studies of the GroEL chaperonin for which it was suggested that bond length and bond angle differences, though subtle, must be detected by the active site (Inobe et al., 2003; Taguchi et al., 2004). Contacts by proteins to the oxygen bridging the β and γ phosphates can also lead to differences in the response of the protein to the various analogs.

We thus conclude that (1) the bacterial enhancer-binding ATPases are exquisitely sensitive to the γ-phosphate moiety, and that in the context of their active site, (2) ADP-BeF_x best mimics the ground state, while (3) ADP-AlF_x mimics the transition state with distinct conformational change between ground- and transition states (seen most clearly at the periphery of the ring), and then between transition to ADP product state (seen most clearly in the thickness of the ring). We propose that rather than by a mechanism involving a single phase of stable contact, these activators interact with σ54 by initially binding in the ATP ground state via lifted GAFTGA loops and then continue and modify the interaction through a significant conformational change that accompanies entering the transition state for ATP hydrolysis. Subsequent

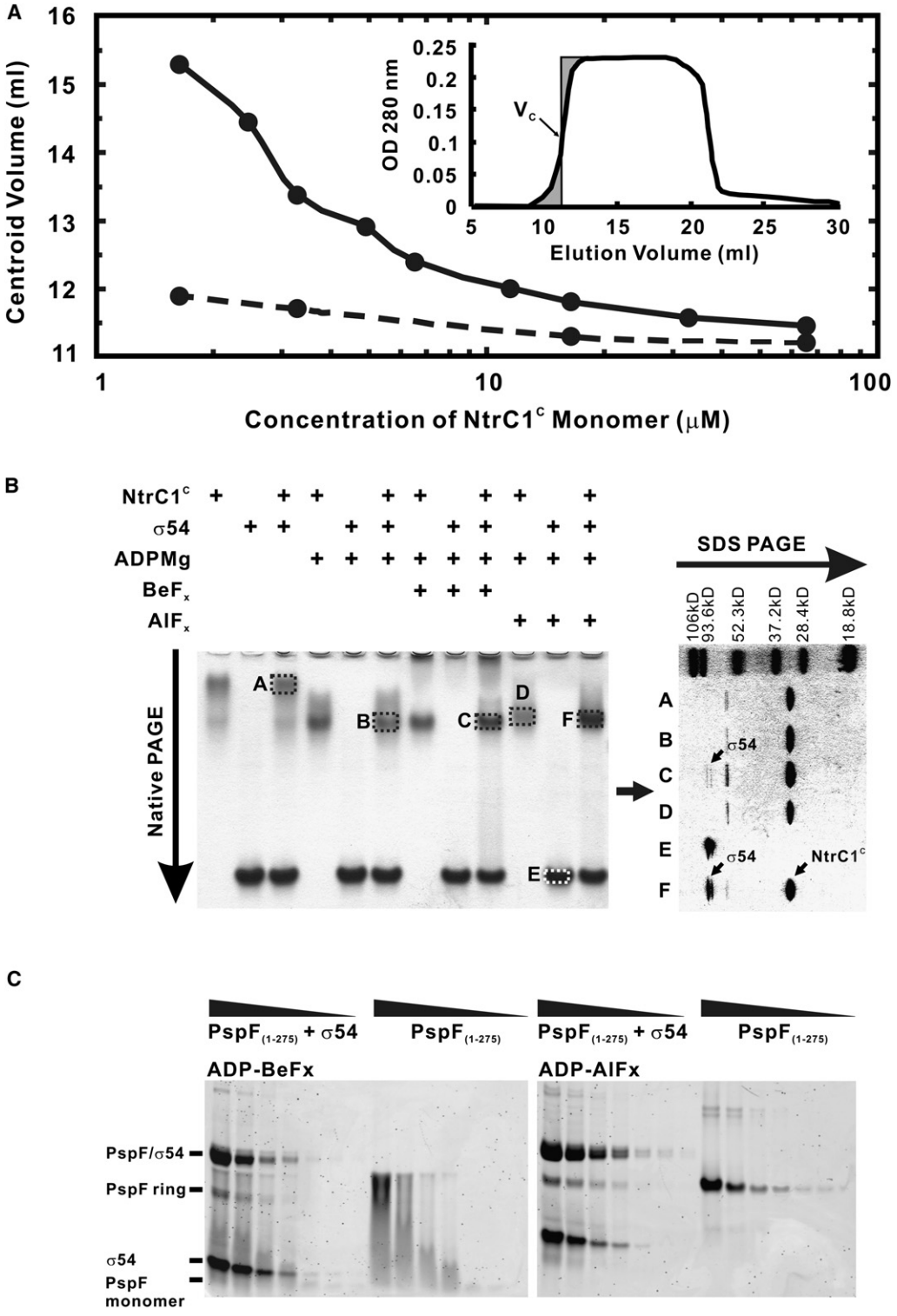

Figure 5. Stability of ATPase Rings and σ54 Complexes Stabilized by ADP-BeF_x versus ADP-AlF_x

(A) Large-zone gel filtration of $NtrC1^C$ in the presence of ADP-BeF_x (solid line) and ADP-AlF_x (dashed line).

(B) The indicated portions of a native gel (lacking ADPMg and metal fluoride) were excised and subjected to SDS-PAGE to assess the presence of $NtrC1^C$ and σ54 after being mixed with ADPMg and BeF_x or AlF_x.

(C) Serial, 2-fold dilutions of 10 μg of $PspF_{(1–275)}$ mixed with 10 μg of σ54 were subjected to native gel electrophoresis with ADPMg-BeF_x or ADPMg-AlF_x present in the sample, buffer, and gel.

release of phosphate and the associated movement of the GAFTGA loop down into the plane of the ATPase, opening of the DNA in the σ54-polymerase complex, and release of σ54 must occur after crossing the transition state, but the order of these later events is not yet clear. Indeed, it has not yet been directly shown that one cycle of hydrolysis is sufficient to render the closed σ54-polymerase complex competent for opening, and it is not known how many subunits in an EBP ring participate in an effective interaction with closed complex. We show that the ATP ground-state analog complex of ATPase and σ54 is less stable than, and therefore distinct from, the transition-state complex. However, like the transition-state complex, the ground-state complex only forms in the presence of an intact GAFTGA loop. We believe these observations demonstrate physiological relevance for the ground-state analog complex. Further study is needed to determine if the initial binding event enables σ54 to alter the −12 promoter region, as previously seen in the ternary complexes of PspF-ADP-AlF_x, polymerase, and promoter (Cannon et al., 2004).

A first glimpse was recently reported of local structural changes that may communicate nucleotide status from the active site of the EBP PspF to its GAFTGA loops in order to direct interaction with σ54 (Rappas et al., 2006). Changes in crystals of the apo form of the PspF ATPase that were soaked in ATP, Mg^{2+}-ATP, ATPγS, or ADP revealed changes in side chain interactions between N64 and E108 (N195 and E239 of $NtrC1^C$), and this was associated with movements of linker loops and secondary structure elements that might link the GAFTGA loop region to the nucleotide status in the active site. Interestingly, $NtrC1^C$ bearing substitutions N195A or E239A has dramatically reduced ATPase activity and, unlike the wild-type protein, form stable rings or rings complexed with σ54 in the presence of ATP (B.C. and B.T.N., unpublished data). The ATP in these complexes is very likely to be in its ground state (especially for the E239A variant, as the E239 equivalent in PspF [E108] is believed to activate water to act as a nucleophile crucial for establishing the transition state for hydrolysis [Rappas et al., 2006]).

While the GAFTGA loops are not visible in the density maps of the PspF crystal structures, the stems on which they sit are reported to move in a way suggesting the loops move up and away from the ring when ATP or AMPPNP is bound (Rappas et al., 2006). Our SAXS/WAXS structures reveal fairly large conformational changes in the GAFTGA loop region that accompany binding of ADP-BeF_x and ADP-AlF_x, and possibly some such movement upon binding AMPPNP. Soaking the crystals with ADP-AlF_x or ADP-BeF_x was not reported (Rappas et al., 2006), and although the lattice clearly did survive soaking with AMPPNP, it is unclear if the AMPPNP preparation used to soak the crystals would support the structural changes that we report here (given our need to repurify the commercial material and lack of information about the AMPPNP preparations that were used to soak the PspF crytals). These considerations probably mean that larger scale motions in response to binding ATP were constrained by the lattice, and thus the changes that were seen may not represent the full range of conformational changes that accompany nucleotide binding, hydrolysis, and P_i release. High-resolution images of activators in nucleotide states that bind σ54 remain elusive. The extension of the GAFTGA loop region from the plane of the ATPase ring that we see at low resolution is consistent with the electron microscopy studies of the ADP-AlF_x-stabilized complex of PspF and σ54 (Rappas et al., 2005). Although density was not apparent for the loops unless contoured at a very low σ threshold, the images suggest that they extend to contact σ54. Such motion of the GAFTGA loops is consistent with the structures we report here. In reconstructions of negative-stain EM images, we saw a similar extension of the GAFTGA loop region when activated NtrC protein is bound to ADP-AlF_x compared to when it is bound to ADP (De Carlo et al., 2006).

Finally, our data indicate that the ATP ground state should couple assembly of ATPase rings and initial binding to σ54, especially in the context of the interaction between an activated, UAS-bound EBP and closed complexes of RNA polymerase with σ54-dependent promoters. It is not yet known if subassemblies (dimers, trimers, etc.) of the ATPase can interact with σ54, or if that is exclusively limited to the fully assembled ring form of the protein. However, looping between UAS and promoter region increases the likelihood of interaction between the DNA-bound ATPase subunits and σ54. Moreover, ring stabilization has been observed for nucleotide binding to several EBPs (Schumacher et al., 2004), and we observe complex ITC data suggesting that partially assembled $NtrC1^C$ fully assembles when σ54 is added to suboptimal concentrations of the ATPase together with ADP-BeF_x (B.C. and B.T.N., unpublished data). Additionally, fragments containing the two-component receiver and ATPase domains of NtrC1 that are activated with BeF_x in the presence of ADP (BeF_3^- bound to the receiver domain, and ADP-BeF_x bound to the ATPase domain) remain only partially assembled into oligomers until the addition of σ54, whereupon they assemble to form heptamer-sized complexes with the target protein (B.C. and B.T.N., unpublished data).

In summary, the SAXS/WAXS-derived, low-resolution structures presented here reveal conformational changes during the nucleotide cycle for the $NtrC1^C$ ATPase. This set of structures led to the identification of novel stable complexes between σ54 and AAA+ ATPase domains of NtrC1, NtrC, and PspF. These complexes are stabilized by the ATP ground-state analog ADP-BeF_x, and, at least for $NtrC1^C$, by highly purified AMPPNP. The structural and molecular biological studies are consistent with substantial reorientations between the subdomains of the ATPase. These reorientations are coupled to an extension of the GAFTGA loop region away from the plane of the ATPase to first make and then alter contact with σ54, which is then released after hydrolysis. The significance of our findings is that ATP binding per se positions the GAFTGA loops such that one or more can engage σ54, albeit less stably than when the active site moves into its

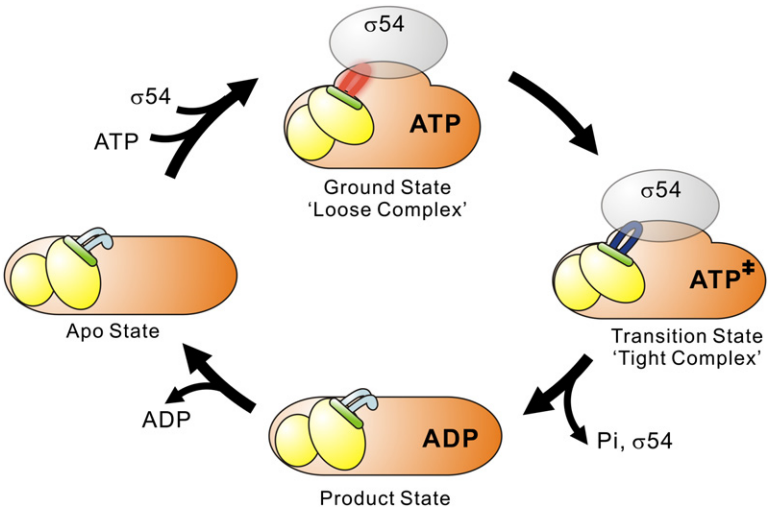

Figure 6. SAS-Based Model of the ATPase Cycle and Interactions with σ54
Binding of ATP extends the GAFTGA loops (one example in red) to permit initial binding to σ54. Conformational changes in the ATPase that accompany entry into the transition state for ATP hydrolysis keep the loops (one example in dark blue) extended but tighten association with σ54 in preparation for its being remodeled. Upon P_i release, the loops (one example in light blue) are retracted from above the ring surface, and contact with σ54 is lost. ADP is then released to repeat the cycle.

hydrolysis transition state. This implies that it is not at the point of ATP hydrolysis that the loop engages with σ54, but likely well before hydrolysis. We thus propose revising the current model for σ54-dependent transcriptional activation to include a distinct step of binding between activator and sigma factor in an ATP ground state that precedes the transition state (Figure 6).

EXPERIMENTAL PROCEDURES

Purification of AMPPNP and ATPγS

100 mg of AMPPNP or ATPγS (Sigma-Aldrich) was purified on Q-HP columns (GE Health Care) using either a 60 to 600 mM gradient of ammonium bicarbonate (pH 8.6), or Tris-HCl (20 mM [pH 8.0]) containing glycerol (5%, w/v) with a linear gradient from 0 to 1 M potassium chloride. Samples in bicarbonate were lyophylized and frozen until use, and those in Tris buffer were used immediately.

Protein Preparations

The following buffers were used: (A) Tris-HCl (50 mM [pH 8.0]), KCl (200 mM), glycerol (5% w/v), tris-2-carboxy-ethylphosphine (TCEP, 5 mM); (B) Tris-HCl (50 mM [pH 8.6]), TCEP (1 mM), $MgCl_2$ (5 mM), ADP (2 mM); (C) Tris-HCl (20 mM [pH 7.8]), KCl (200 mM), glycerol (5% w/v), TCEP (5 mM), ADP (2 mM), $MgCl_2$ (5 mM), metal fluoride (10 mM NaF and 5 mM $BeCl_2$ or 1 mM $AlCl_3$); (D) Tris-HCl (20 mM [pH 7.8]), KCl (200 mM), glycerol (5% w/v), $MgCl_2$ (5 mM), ADP (1 mM), metal fluoride (20 mM NaF and 5 mM $BeCl_2$ or 200 μM $AlCl_3$); and (E) HEPES (200 mM [pH 7.8]), KCl (200 mM), trehalose (5% w/v), ADP (1 mM), $MgCl_2$ (5 mM), NaF (1 mM), and $BeCl_2$ (200 μM). $NtrC1^C$ from *A. aeolicus*, σ54 (with His6 tag) from *Klebsiella pneumoniae*, $PspF_{(1–275)}$ ATPase (His6 tag removed with thrombin) from *E. coli*, and activated NtrC (S160F, 3Ala) from *Salmonella typhimurium* were prepared as described (De Carlo et al., 2006; Lee et al., 2003; Rappas et al., 2005). Substitution T217A was introduced into $NtrC1^C$ using the QuikChange Multi Site-Directed Mutagenesis Kit (Stratagene) with oligo 5′-GAAAAGGGAGCCTTCGCGGGAGCAGTATCTTCC-3′ (Integrated DNA Technology) and confirmed by DNA sequencing. Purified proteins were stored in buffer A or that plus 25% glycerol at −60°C until thawed once for data collection. Dynamic light scattering was performed at 21°C with a DynaPro (Protein Solutions) instrument on $NtrC1^C$ samples before and after thawing, yielding a single species of 6.1 nm radius (229 Kd mwt) with 22.6% polydispersity. Rarely, less than 0.1% of the material was present as an aggregate, which was removed by overnight incubation at 4°C.

Assays for Nucleotide Binding and Hydrolysis, and for σ54-ATPase Complexation

$NtrC1^C$ (3 μM, buffer B) was titrated to final AlF_x concentrations of 0 to 3.5 mM. Fluorescence was measured at 25°C for 1 s with excitation and emission wavelengths of 280 and 340 nm, respectively, using a SPEX Fluoromax-3 spectrofluorometer (Horiba Jobin Yvon, Edison, NJ). Background changes in ADP fluorescence due to AlF_x binding, measured by repeating the titration without $NtrC1^C$, were subtracted from each data point. The data were analyzed in terms of a Hill plot, $\log(Y/(1 - Y)) = \log[ADP - AlF_x]$, where Y is the normalized saturation value. Isothermal titration calorimetry was performed at 25°C with an MCS-ITC microcalorimeter (MicroCal, Inc., Northampton, MA). The 1.4 ml reaction cell containing $NtrC1^C$ (25 μM, buffer B lacking ADP and $MgCl_2$). After subtracting background heat released upon dilution, data were graphed and fit to a one-site binding model using the program MicroCal-ORIGIN. Hydrolysis of ATP, ATPγS, and AMPPNP was measured by determining the concentration of free P_i, or thiophosphate, essentially as described (Chen et al., 2003).

Small-zone size-exlcusion chromatography was performed in buffer D, or similar buffer lacking ADP-metal fluoride but containing other nucleotide. Twelve milligrams of $NtrC1^C$, $PspF_{(1–275)}$, or full-length NtrC (S160F, 3Ala; activated with 200 μM Mg^{2+}/BeF_3^-) and 12 mg of σ54 were premixed in buffer lacking ADP and $MgCl_2$. These were concentrated to 1 ml by centrifugation (Amicon Ultra 15, 10,000 MWCO) before being mixed 1:1 with complete buffer and further concentrated to 0.5 ml (final concentrations ranging between 30 and 35 mg/ml). Samples (25–100 μl) were injected onto a 24 ml Superdex200 (Pharmacia) column and chromatographed at 0.5 ml/min, collecting single-drop fractions for SDS-PAGE analysis using SYPRO orange and a Typhoon Fluorimager (Molecular Dynamics), or Comassie Blue and a Personal Laser Densitometer (Molecular Dynamics). For ATPγS and AMPPNP, 25 μl samples were injected onto a 2.4 ml column and developed at a flow rate of 30 μl/min. Average pseudo partition coefficients were calculated as: $K_{av} = (V_e - V_o)/(V_t - V_o)$, where V_e, V_o, and V_t are the elution, void, and total volumes, respectively. For large-zone experiments, mixtures of $NtrC1^C$ and σ54 were diluted to 10 ml in buffer D (modified to contain 1 mM instead of 200 μM $AlCl_3$) and passed through a 0.1 μm filter before being applied to a 24 ml Superdex200 column at 0.5 ml/min. The centroid volume V_c was found using numerical integration. Native gel electrophoresis was performed as described (Chaney et al., 2001), but on wet ice. For $NtrC1^C$, excised portions of the native gel were subjected to SDS-PAGE after incubation in SDS-PAGE loading buffer for 30 min. To include ADP-BeF_x or ADP-AlF_x, the pH of buffer and gel was brought to 7.5 with HCl, and 0.5 mM ADP, 0.5 m $MgCl_2$, 6.5 mM NaF, and 0.5 mM $AlCl_3$ or $BeCl_2$ were added.

SAXS/WAXS Data Collection and Processing

Experiments were done on the Biophysics Collaborative Access Team (BioCAT) undulator beamline 18-ID at the Advanced Photon Source, Argonne National Lab (Fischetti et al., 2004). Thawed protein solutions were incubated overnight at 4°C and then mixed with small aliquots of freshly prepared AMPPNP, ATPγS, ADP, or ADP previously mixed with stock solutions of $BeCl_2$ or $AlCl_3$ and NaF (Sigma Aldrich). Protein was pipetted first into nucleotide, then metal fluoride if appropriate, and finally into $MgCl_2$, achieving 5 mM concentration of nucleotides, $MgCl_2$, $BeCl_2$, and $AlCl_3$, and 20 mM NaF. Samples were passed through a 0.1 μm filter and pumped through a 1.5 mm wide quartz capillary at 12.5 μl/s for exposure to focused X-rays (12 keV, 2×10^{13} photons/s) for an average of 0.600 ± 0.005 s. A 5×9 cm charge-coupled device (CCD) detector (Phillips et al., 2002) located 2.78 m or 2.49 m (SAXS) or 0.24 m (WAXS) from the sample collected 2D scattering patterns. Averaged scattering from buffer alone was subtracted from averaged scattering of protein solution. Radiation damage, assessed by Rg calculations using the Guinier approximation, was effectively minimized by including 5% glycerol (Kuwamoto et al., 2004), 5 mM TCEP and flowing at 12.5 μl/s (Fischetti et al., 2003) (Figure S9). Distance distribution functions calculated with GNOM (Svergun, 1992) were used with GASBOR (Svergun et al., 2001) on the LionXL computer cluster at Penn State to obtain eight independent, P7-symmetric solution structures (Figure S5 and Document S2). These were analyzed for similarity using the "normalized spatial discrepancy" (NSD) of SUPCOMB (Kozin and Svergun, 2001). The ensemble of superimposed solutions was then averaged and filtered with DAMAVER (Volkov and Svergun, 2003) to generate a model most likely to be correct (those shown in Figure 3 are for the p(R) function derived at the optimal Total Score from GNOM—153 Å for Apo; 158 Å for commercial AMPPNP; 168 Å for repurified AMPPNP; 157 Å for ATPγS; 180 Å for ADP-BeF_x; 199 Å for ADP-AlF_x; and 165 Å for ADP). Images of the ab initio models were made either by using POV-RAY (www.povray.org) and DeepView (Guex and Peitsch, 1997), or Discovery Studio Visualizer (Accelrys). Composite figures or animations were made using Photoshop (Adobe) or ImageReady (Adobe).

Electron Microscopy

$NtrC1^C$ (10 mg/ml, buffer A) was exchanged to buffer E and mixed 1:1 with 2× buffer supplemented with 0.01%–0.25% glutaraldehyde, incubated 15 min at 21°C, quenched with 10 μl of Tris/glycine (100 mM final concentration), and subjected to SDS-PAGE (Figure S3). Size-exclusion chromatography fractions corresponding to the oligomeric form were collected in buffer containing ADP-BeF_x, diluted 15-fold, and adsorbed onto a freshly glow-discharged carbon film supports mounted on 200-mesh EM grids. After 1 min the samples were stained 30 s with uranyl-acetate (3%), blotted, and air dried. Electron micrographs were collected at 0° degrees in a Tecnai 12 electron microscope (FEI) operated at 120 kV, with calibrated magnification of 49,687× and defocus ranging from 1.0 to 1.5 μm. Astigmatism- and drift-free micrographs were digitized using a Nikon SuperCoolscan ED8000 scanner at 2.56 Å/pixel (at the specimen scale). Particles were semiautomatically picked and extracted from the micrographs using EMAN (Ludtke et al., 1999). Using SPIDER (Frank et al., 1996), 125 by 125 pixel windows were passed through a 22 Å Fermi low-pass filter to remove all information beyond the first CTF zero, but CTF correction was not otherwise applied. Initial class averages, obtained with translational alignment but without rotational alignment or symmetry, were subject to 4 cycles of multivariate statistical analysis using 16 eigenfactors and avoiding 7-fold symmetry bias, followed by hierarchical ascendant classification using Ward's criterion (Ward, 1963) and 2D alignment (both rotation and translation).

Supplemental Data

Supplemental Data include a table summarizing the currently available high resolution structures of ADP-BeF and ADP-AlF; nine figures providing detailed information about experimental methods and modeling from SAXS/WAXS data; six PDB files containing all derived models aligned with each other, the averaged filtered model, and the crystal structure of ADP-bound NtrC1C ATPase (PDB 1NY6); and two movies illustrating the inferred conformational changes that occur during the hydrolysis cycle. These supplemental materials can be found at http://www.structure.org/cgi/content/full/15/4/429/DC1/.

ACKNOWLEDGMENTS

We thank Dmitri Svergun and Maxim Petoukhov for advice and modifying GASBOR to accommodate P7 symmetry, and Sydney Kustu for making useful comments on the manuscript. This work was funded by NSF, Huck Institute (Penn State), and NIH grants to B.T.N., an NIH grant to D.E.W., and a DOE grant to E.N. and B.T.N. E.N. is a Howard Hughes Medical Institute Investigator. Use of the Advanced Photon Source was supported by the DOE under contract number W-31-109-ENG-38, and the BioCAT is an NIH-supported research center.

Received: October 3, 2006
Revised: November 1, 2006
Accepted: February 22, 2007
Published: April 17, 2007

REFERENCES

Buck, M., Bose, D., Burrows, P., Cannon, W., Joly, N., Pape, T., Rappas, M., Schumacher, J., Wigneshweraraj, S., and Zhang, X. (2006). A second paradigm for gene activation in bacteria. Biochem. Soc. Trans. *34*, 1067–1071.

Cannon, W., Schumacher, J., and Buck, M. (2004). Nucleotide-dependent interactions between a fork junction-RNA polymerase complex and a AAA+ transcriptional activator protein. Nucleic Acids Res. *32*, 4596–4608.

Chabre, M. (1990). Aluminofluoride and beryllofluoride complexes: new phosphate analogs in enzymology. Trends Biochem. Sci. *15*, 6–10.

Chaney, M., Grande, R., Wigneshweraraj, S.R., Cannon, W., Casaz, P., Gallegos, M.T., Schumacher, J., Jones, S., Elderkin, S., Dago, A.E., et al. (2001). Binding of transcriptional activators to sigma 54 in the presence of the transition state analog ADP-aluminum fluoride: insights into activator mechanochemical action. Genes Dev. *15*, 2282–2294.

Chen, B., Guo, Q., Guo, Z., and Wang, X. (2003). An improved activity assay method for arginine kinase based on a ternary heteropolyacid system. Tsinghua Sci. Technol. *8*, 422–427.

Dago, A.E., Wigneshweraraj, S.R., Buck, M., and Morett, E. (2007). A role for the conserved GAFTGA motif of AAA+ transcriptional activators in sensing promoter DNA conformation. J. Biol. Chem. *282*, 1087–1097.

De Carlo, S., Chen, B., Hoover, T.R., Kondrashkina, E., Nogales, E., and Nixon, B.T. (2006). The structural basis for regulated assembly and function of the transcriptional activator NtrC. Genes Dev. *20*, 1485–1495.

Doucleff, M., Chen, B., Maris, A.E., Wemmer, D.E., Kondrashkina, E., and Nixon, B.T. (2005). Negative regulation of AAA+ ATPase assembly by two component receiver domains: a transcription activation mechanism that is conserved in mesophilic and extremely hyperthermophilic bacteria. J. Mol. Biol. *353*, 242–255.

Fischetti, R.F., Rodi, D.J., Mirza, A., Irving, T.C., Kondrashkina, E., and Makowski, L. (2003). High-resolution wide-angle X-ray scattering of protein solutions: effect of beam dose on protein integrity. J. Synchrotron Radiat. *10*, 398–404.

Fischetti, R., Stepanov, S., Rosenbaum, G., Barrea, R., Black, E., Gore, D., Heurich, R., Kondrashkina, E., Kropf, A.J., Wang, S., et al. (2004). The BioCAT undulator beamline 18ID: a facility for biological non-crystalline diffraction and X-ray absorption spectroscopy at the Advanced Photon Source. J. Synchrotron Radiat. *11*, 399–405.

Frank, J., Radermacher, M., Penczek, P., Zhu, J., Li, Y., Ladjadj, M., and Leith, A. (1996). SPIDER and WEB: processing and visualization of images in 3D electron microscopy and related fields. J. Struct. Biol. *116*, 190–199.

Glatter O. and Kratky O., eds. (1982). Small-Angle X-Ray Scattering (London: Academic Press).

Guex, N., and Peitsch, M.C. (1997). SWISS-MODEL and the Swiss-PdbViewer: an environment for comparative protein modeling. Electrophoresis *18*, 2714–2723.

Inobe, T., Kikushima, K., Makio, T., Arai, M., and Kuwajima, K. (2003). The allosteric transition of GroEL induced by metal fluoride-ADP complexes. J. Mol. Biol. *329*, 121–134.

Kozin, M.B., and Svergun, D.I. (2001). Automated matching of high- and low-resolution structural models. J. Appl. Cryst. *34*, 33–41.

Kuwamoto, S., Akiyama, S., and Fujisawa, T. (2004). Radiation damage to a protein solution, detected by synchrotron X-ray small-angle scattering: dose-related considerations and suppression by cryoprotectants. J. Synchrotron Radiat. *11*, 462–468.

Lee, S.-Y., DeLaTorre, A., Yan, D., Kustu, S., Nixon, B.T., and Wemmer, D.E. (2003). Regulation of the transcriptional activator NtrC1: structural studies of the regulatory and AAA+ ATPase domains. Genes Dev. *17*, 2552–2563.

Ludtke, S.J., Baldwin, P.R., and Chiu, W. (1999). EMAN: semiautomated software for high-resolution single-particle reconstructions. J. Struct. Biol. *128*, 82–97.

Nenortas, E., and Beckett, D. (1994). Reduced-scale large-zone analytical gel filtration chromatography for measurement of protein association equilibria. Anal. Biochem. *222*, 366–373.

Phillips, W.C., Stewart, A., Stanton, M., Naday, I., and Ingersoll, C. (2002). High-sensitivitiy CCD-based X-ray detector. J. Synchrotron Radiat. *9*, 36–43.

Rappas, M., Schumacher, J., Beuron, F., Niwa, H., Bordes, P., Wigneshweraraj, S.R., Keetch, C.A., Robinson, C.V., Buck, M., and Zhang, X. (2005). Structural insights into the activity of enhancer-binding proteins. Science *307*, 1972–1975.

Rappas, M., Schumacher, J., Niwa, H., Buck, M., and Zhang, X. (2006). Structural basis of the nucleotide driven conformational changes in the AAA+ domain of the transcription factor PspF. J. Mol. Biol. *357*, 481–492.

Rombel, I., Peters-Wendisch, P., Mesecar, A., Thorgeirsson, T., Shin, Y.K., and Kustu, S. (1999). MgATP binding and hydrolysis determinants of NtrC, a bacterial enhancer-binding protein. J. Bacteriol. *181*, 4628–4638.

Schumacher, J., Zhang, X., Jones, S., Bordes, P., and Buck, M. (2004). ATP-dependent transcriptional activation by bacterial PspF AAA+ protein. J. Mol. Biol. *338*, 863–875.

Svergun, D.I. (1992). Determination of the regularization parameter in indirect-transform methods using perceptual criteria. J. Appl. Cryst. *25*, 495–503.

Svergun, D.I., and Koch, M.H.J. (2003). Small-angle scattering studies of biological macromolecules in solution. Rep. Prog. Physics *66*, 1735–1782.

Svergun, D.I., Petoukhov, M.V., and Koch, M.H.J. (2001). Determination of domain structure of proteins from X-ray solution scattering. Biophys. J. *80*, 2946–2953.

Taguchi, H., Tsukuda, K., Motojima, F., Koike-Takeshita, A., and Youshida, M. (2004). BeF(x) stops the chaperonin cycle of GroEL-GroES and generates a complex with double folding chambers. J. Biol. Chem. *279*, 45737–45743.

Valdes, R., and Ackers, G.K. (1979). Study of protein subunit association equilibria by elution gel chromatography. Methods Enzymol. *61*, 125–142.

Volkov, V.V., and Svergun, D.I. (2003). Uniqueness of *ab initio* shape determination in small-angle scattering. J. Appl. Cryst. *36*, 860–864.

Wang, L., and Gralla, J.D. (2001). Roles for the C-terminal region of sigma 54 in transcriptional silencing and DNA binding. J. Biol. Chem. *276*, 8979–8986.

Wang, Y.-K., Park, S., Nixon, B.T., and Hoover, T.R. (2003). Nucleotide-dependent conformational changes in the σ54-dependent activator DctD. J. Bacteriol. *185*, 6215–6219.

Ward, J.H., Jr. (1963). Hierarchical grouping to optimize an objective function. J. Am. Stat. Assoc. *58*, 236–244.

